Sensitivity of Novel Micro-AlN/GaN/AlN Quantum Well Hall Sensors

Satish Shetty, Fernando Maia de Oliveira, Yuriy I. Mazur, H. Alan Mantooth, *Fellow, IEEE*, and Gregory J. Salamo

***Abstract*—We have grown AlN/gallium nitride (GaN)/AlN heterostructures by molecular beam epitaxy (MBE) and fabricated Hall sensors. In a comparison with fabricated AlGaN/AlN/GaN Hall sensors, we find that the AlN/GaN/AlN quantum well (QW) Hall sensors have higher sensitivity under constant current bias. In addition, the application of a gate voltage shows a further increase in the Hall sensitivity from 3.6 to 6.1 $VW^{-1}T^{-1}$, without a significant change in the operating parameters. This is because the gate voltage restricted the current flow resulting in an increase carrier velocity and electric field at precisely the Hall measurement site while keeping the device applied power approximately the same.**

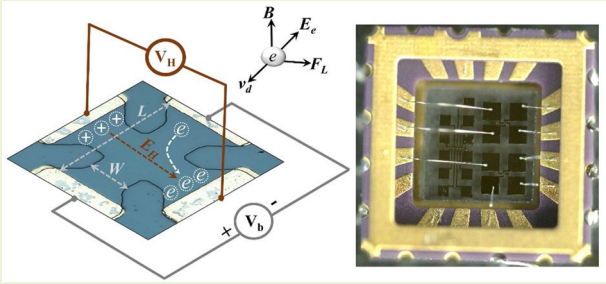

***Index Terms*—Gallium nitride (GaN), heterostructure, high electron mobility transistor (HEMT), micro-Hall sensor, molecular beam epitaxy (MBE), offset voltage, quantum well (QW).**

I. Introduction

HALL effect sensors have been widely used for many years for magnetic pole position detection and contactless switching applications [1]. Such magnetic sensors, when integrated into CMOS technology, have also been very effective for monitoring currents in low-power electronic circuits [2], [3], [4], [5], [6]. However, increasing power demands, coupled with the need for smaller size and weight for high power units, have created a market for GaN and silicon carbide (SiC) high electron mobility transistors (HEMTs) [7], which allow for modern power systems to be designed at much higher power densities and operating temperatures [8], [9], [10], [11]. As a result, there is a corresponding need for Hall sensors for higher power current sensing that can also tolerate the same higher operating temperatures. The GaAs material system has for many years [12], [13], [14] been an effective material system for the fabrication of the Hall sensor conductive channel, followed by processing and adding metal contacts to enable the measurement of the Hall voltage sensor signal. However, the GaAs material system Hall sensors prove to have a limited upper temperature range on the order of 200 °C [15]. The wide bandgap semiconductors gallium nitride (GaN), gallium oxide (Ga_2O_3), and SiC are considered potential material systems for high-temperature device application [16], [17]. Significant progress has been made in recent years on the development of GaN quantum well (QW)-based radio frequency (RF), high-voltage, and high-temperature power electronic devices [17], [18], [19]. These advancements are expected to have a tremendous impact on various areas, including all-electric vehicles, high-voltage/high-power electronics, and devices that operate at high speeds and frequencies. However, it is crucial to monitor the high operating currents and temperatures that can potentially result in catastrophic failure.

One approach to fabricate Hall sensors to be used in high-power devices and high-temperature environments is to use the same GaN material system for the sensor that is used for fabricating high-power HEMTs [1], [20]. This approach has the additional advantage of monolithic integration of transistor and sensor on the same chip. In a previous article, we demonstrated a high-sensitivity, robust, high-temperature micro-Hall sensor using the GaN material system grown by molecular beam epitaxy (MBE) [20], [21], [22], [23]. The sensor was based on the formation of a 2-D electron gas (2DEG) at the AlGaN/GaN heterostructure interface [24], [25] and on the wider bandgap feature of the AlGaN and GaN materials over GaAs materials, allowing it to tolerate higher operating temperature environments. The novelty of the sensor was that it could simultaneously determine both current and temperature as well as utilize a new method to separate out

Manuscript received 24 November 2023; revised 21 December 2023; accepted 21 December 2023. Date of publication 3 January 2024; date of current version 13 February 2024. This work was supported by the Army Research Laboratory (ARL) under Grant W911NF-21-2-0231, towards the development of a SiC CMOS process for advanced integration. The associate editor coordinating the review of this article and approving it for publication was Prof. Kai Wu. *(Corresponding author: Satish Shetty.)*

Satish Shetty, Fernando Maia de Oliveira, Yuriy I. Mazur, and Gregory J. Salamo are with the Institute for Nanoscience and Engineering, University of Arkansas, Fayetteville, AR 72701 USA (e-mail: ss110@uark.edu; fmaiade@uark.edu; ymazur@uark.edu; salamo@uark.edu).

H. Alan Mantooth is with the Department of Electrical Engineering, University of Arkansas, Fayetteville, AR 72701 USA (e-mail: mantooth@uark.edu).

Digital Object Identifier 10.1109/JSEN.2023.3347687

the troubling offset voltage from the produced sensor Hall voltage [20].

In this article, we build on past results and investigate gated AlN/GaN/AlN QWs fabricated as Hall sensors. The QWs were grown by MBE on an AlN template, which consists of a sapphire substrate with a metal–organic chemical vapor deposition grown, 1-μm-thick AlN semi-insulating layer. The AlN/GaN/AlN QWs have been investigated before and shown the tunable 2DEG density by changing the GaN QW thickness and high-frequency filed-effect transistor performance with cutoff frequency <100 GHz [26], [27] and therefore which are good reason to believe they are good candidates to explore Hall sensors application. The use of AlN/GaN interface has the advantages of a high breakdown voltage and larger band offset compared to $Al_{0.20}Ga_{0.80}N$/GaN as well as a larger difference of spontaneous and piezoelectric polarization [28], [29], [30] across the heterojunction. Hence, the AlN/GaN/AlN-QW-based Hall sensors can have potential advantages in achieving high carrier confinement and low sheet resistance, associated with the 2DEG that forms at the AlN/GaN interface. It also has the potential advantage of integration with high-power transistors on a single-chip AlN platform, which is preferred over GaN due to higher thermal conductivity. Our study also demonstrates a sensitivity enhancement that is observed by applying a gate voltage at the spatial location of the Hall signal measurement, restricting the 2DEG cross-sectional area, resulting in an increase carrier velocity and electric field at only the Hall measurement site, while keeping the device applied voltage and bias current approximately the same.

For the investigation, we have grown several AlN/GaN/AlN heterostructures by MBE and fabricated Hall sensors while varying QW thickness and measuring the Hall signal, carrier concentration, and carrier mobility. In a comparison with fabricated AlGaN/1.3-nm AlN/GaN Hall sensors, we find that the AlN/GaN/AlN QW Hall sensors have higher sensitivity for fixed current bias while the added use of a gate voltage shows a dramatic increase in the Hall sensitivity without a significant change in the operating parameters.

In Section II, we give the experimental details of both the equipment and approach utilized, while Section III describes and discusses the corresponding observations. Section IV brings the observations to a conclusion that the use of a gate can improve the performance of all Hall sensors.

II. Experimental Details

AlN/GaN/AlN QW Fig. 1 grown by MBE on top of an AlN template was used to fabricate and study Hall devices. The QWs were grown on the template using a Veeco Gen II RF nitrogen plasma cell. The active device structure consists of a 50-nm AlN buffer, followed by a GaN and AlN, forming a QW. Eight QW device structures were studied, each with a different QW thicknesses t including, 2, 4, 8, 10, 15, 20, 30, and 40 nm. The structure is depicted in Fig. 1(a). The AlN buffer layer, 4-nm top AlN barrier, and cap 1.5-nm GaN thicknesses, remained the same for all Hall structures. Prior to the growth process, the template was prepared following the detailed preparation described elsewhere [31], [32], [33], [34]. For all samples, the substrate temperature was

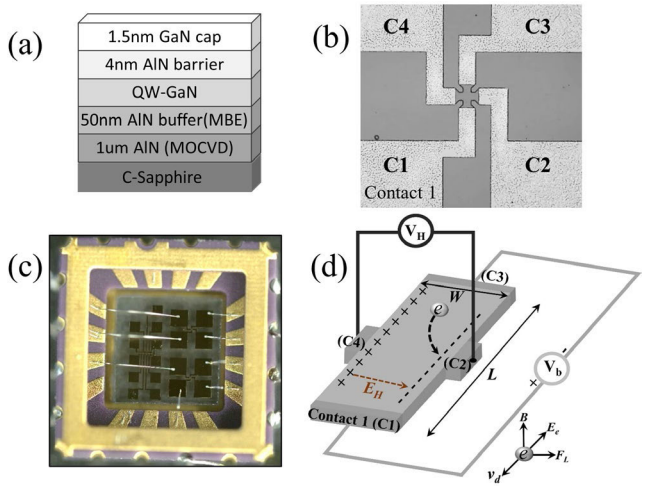

Fig. 1. (a) Cross-sectional growth diagram of AlN/GaN/AlN QW Hall sensor. (b) Plan view of Greek-cross Hall sensor device. (c) Micro-Hall sensor located in chip carrier. (d) Typical Hall sensor, which produces a Hall voltage V_H as a function of magnetic field B.

maintained at 794 °C and nitrogen was supplied from the nitrogen plasma cell with power maintained at 350 W and nitrogen flow rate at 0.5 standard cubic centimeter per minute (sccm), which corresponded to a 4-nm/min deposition rate. The chamber pressure remained stable at 3.25×10^{-6} torr throughout the growth process, and the growth mode and growth rate were monitored by in situ reflection high-energy electron diffraction (RHEED). Prior to processing for device fabrication, the sample was dipped in HCl solution for 20 min to remove any possible excess Ga metal droplets from the surface. A Cl-based inductively coupled plasma (ICP) dry etch technique was employed to form "Greek-cross" Hall devices, with a corresponding mesa etch depth of ~200 nm. Prior to adding ohmic contacts by deposition, a selective premetallization plasma etching procedure was conducted producing an etch depth of about 2 nm only in the contact region of mesa structure. The ohmic contacts were formed with a Ti (30 nm)/Al (200 nm)/Ni (50 nm)/Au (100 nm) metal stack deposited by e-beam evaporation, followed by rapid thermal annealing (RTA) at 750 °C for 30 s to enhance diffusion. The ohmic contact pad dimension is 500 × 500 μm at the wire bond site, and at the 2DEG contact site, it is about ~20 μm wide. Each chip, containing two Greek-cross Hall sensors, was mounted on a nonmagnetic chip carrier for electrical characterization [Fig. 1(b) and (c)].

These two Hall devices on a single chip gave equal performance. Practically, the second sensor acted as a backup sensor. The Hall sensor response as a function of temperature and magnetic field, operating in the constant current or constant voltage bias mode, was characterized using an MMR Technologies H-50 Hall Effect system.

III. Results and Discussion

The schematic representation of the Hall Effect is shown in Fig. 1(d). In this figure, V_b is the applied bias voltage applied across contacts C1 and C3 that create a bias current I_b or charge carriers that move through the semiconductor at a drift velocity v_d. A magnetic field B was applied perpendicular to the sample. As a result, charge carriers transporting across the semiconductor experience a force to the side which is

compensated by developing E field in the plane of the sample and perpendicular to the conducting path. At equilibrium, the electric field produces a force on the charge carriers that balance the force due to the magnetic field. The developing electric field is responsible for a sensor signal or Hall voltage V_H that develops across metal contacts, C2 and C4, in the presence of the magnetic field. The Hall voltage of a Hall sensor is primarily dependent on the carrier charge (electrons in this case), drift velocity $\boldsymbol{v_d}$, and component of the magnetic field perpendicular to the plane of the device B, described by (1) and (2), and consequently is dependent on the material carrier mobility, shown in (3). Here, q is the carrier elemental charge, w is the width of the etched conductive channel, and E_H is the Hall electric field formed due to charge accumulation at contacts C2 and C4 at equilibrium [Fig. 1(d)]

$$qv_dB = qE_H \tag{1}$$

therefore

$$V_H = wv_dB. \tag{2}$$

These equations are basically determined at equilibrium from the balance of the electrical and magnetic forces on every charge carrier forming the bias current. Likewise, the drift velocity can be written by defining the carrier mobility $\boldsymbol{\mu}$ as

$$v_d = \mu E_b \tag{3}$$

where $\boldsymbol{E_b}$ is the applied bias electric field, which for a given bias current can be used in (3) as

$$I_b = Aq(n_s/t)\mu E_b \tag{4}$$

where $\boldsymbol{A}$ is the cross-sectional area for the bias current. Therefore

$$V_H = wv_dB = wI_bB/(Aqn) = I_bB/(qn_s) \tag{5}$$

where n is the 3-D carrier density and n_s is the carrier sheet density or the 3-D carrier density divided by the effective thickness t of the current carrying region. Based on (4) and (5), the Hall effect is typically employed to determine the mobility, carrier sign, and sheet carrier density, using the bias current and measured Hall voltage. For example, the carrier sheet density and mobility for AlN/GaN/AlN QW Hall sensors of thicknesses 40, 30, and 20 nm are shown in Fig. 2(a) and (b). The results for both the carrier mobility and sheet carrier density are consistent with results from previous investigations [26]. For example, Fig. 2(a) indicates a reduction of sheet carrier density as the thickness of the GaN QW is reduced from 40 to 20 nm, but little change between 40 and 30 nm. This behavior is expected based on the 2DEG that forms at the AlN/GaN interface [26]. For the 40- and 30-nm QW, the 2DEG at the AlN/GaN interface is on the order of 10–20 nm and its confinement is not significantly affected by the change in QW width from 40 to 30 nm. However, we can expect an impact on carrier confinement and corresponding sheet density for QWs with a thickness below 20 nm.

Likewise, we also found that the residual strain in the GaN QW of AlN/GaN/AlN heterostructure was only slightly affected for QW thicknesses above 20 nm but significantly affected for QWs at or below 20 nm as determined from Raman measurements, shown in Fig. 3(a)–(c). The E_2 (high)

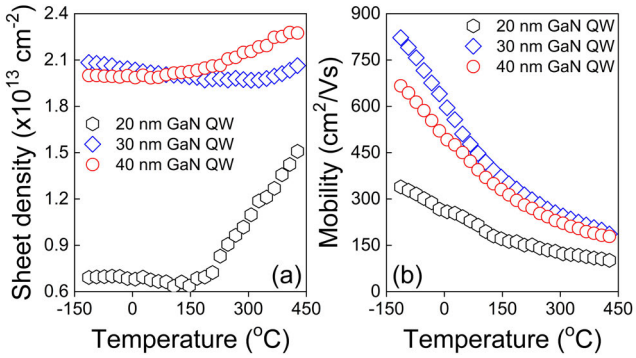

Fig. 2. Measured (a) carrier sheet density and (b) carrier mobility as a function of temperature for three GaN QWs (20, 30, and 40 nm), respectively.

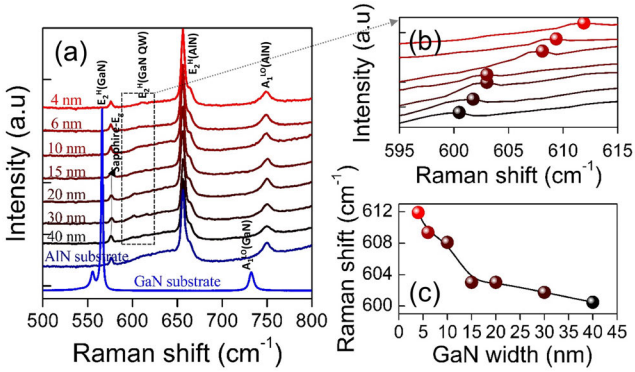

Fig. 3. (a) Raman spectra acquired for AlN/t-GaN/AlN QW [QW thicknesses (t) = 4, 6, 10, 15, 20, 30, and 40 nm] structures grown on AlN/sapphire substrates, the reference sample Raman spectra acquired for 1-μm AlN/sapphire (navy color), and bulk GaN (blue color), respectively. (b) Zoomed-in view showing the E_2 (high) phonon mode of GaN QW. (c) Plot of the shift in E_2 (high) Raman peak position as a function of GaN QW thickness.

phonon mode is particularly sensitive to residual in-plane strain [27], [35]. The data show that an increasing Raman frequency shift is observed as the thickness of the GaN QW is reduced, indicating that the corresponding compressive strain is increased with decreasing thickness. Since the GaN cap layer is very thin (1.5 nm), the Raman signal primarily originates from the GaN quantum well (QW) structure.

The observed change in the compressive strain field with GaN QW thickness has a direct correlation with the sheet carrier density. The direction of the piezoelectric polarization in the GaN QW adds to the spontaneous polarization with tensile strain and is opposite to the spontaneous polarization under compressive strain. Therefore, we can expect an increase in piezoelectric polarization and a decrease in net polarization as the compressive strain increases with lower QW thickness. The compressive strain transitions from high to low at around 20–30 nm as observed by Raman results and other reports [26]. The significance is that a lower net polarization results in a lower 2DEG sheet density. By using Raman analysis, we were able to correlate the observed change in sheet density with respect to QW thickness and corresponding influence of compressive strain field. Note that below 15-nm GaN QW thickness, there is a significant reduction of sheet density leading to a nonconducting behavior of Hall device, therefore limiting Hall measurements on those devices. Our analysis is therefore focused on QW thickness for 20 nm and above.

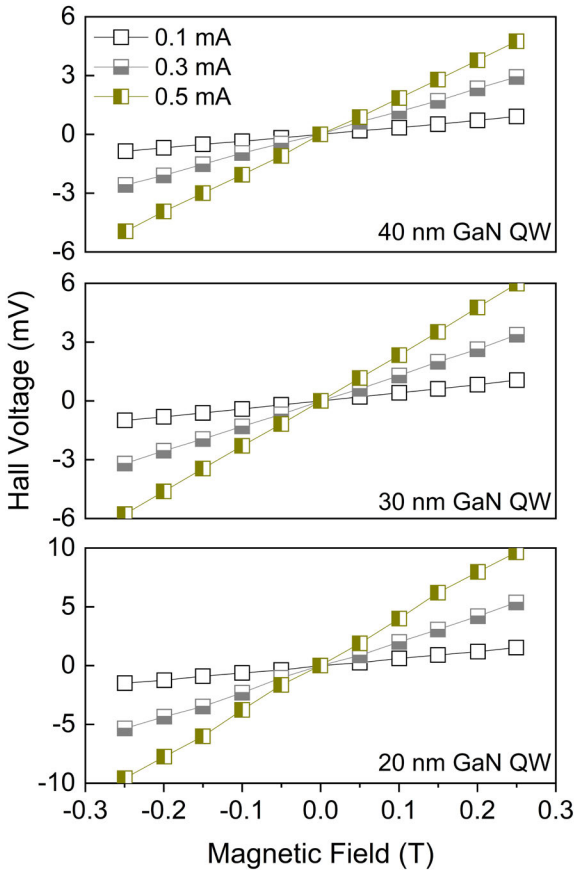

Fig. 4. AlN/GaN/AlN QW micro-Hall sensors have a linear response to magnetic field, in the range from −0.25 to 0.25 T magnetic field, over a wide range of constant bias current (top color code), for the 40-, 30-, and 20-nm QWs at room temperature.

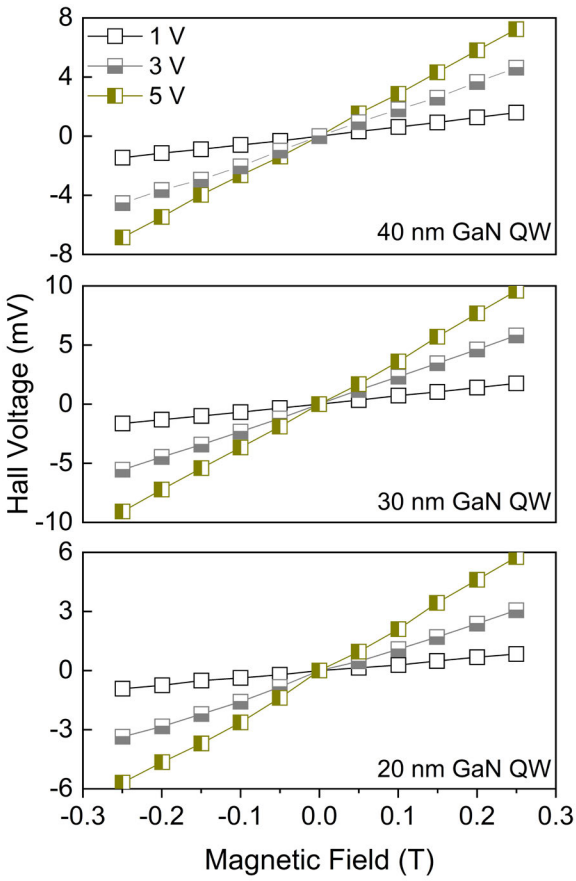

Fig. 5. AlN/GaN/AlN QW micro-Hall sensors have a linear response to magnetic field, in the range from −0.25 to 0.25 T magnetic field, over a wide range of constant bias voltage (top color code), for the 40-, 30-, and 20-nm QWs at room temperature.

For a practical Hall sensor, the Hall voltage versus magnetic field relationship must remain linear over a wide temperature range of magnetic field strength. As shown in Figs. 4 and 5, the AlN/GaN/AlN QW Hall sensors of thicknesses 40, 30, and 20 nm have a linear response to a changing magnetic field in the range from −0.25 to 0.25 T, when biased using either a constant current bias or a constant voltage bias, respectively.

In addition, the measured Hall voltage versus bias current for fixed 0.1 T magnetic field at room temperature is shown in Fig. 6 for the 40-, 30-, and 20-nm QWs, respectively. The Hall voltage signal is seen to get progressively higher with decreased thickness as expected due to the decreased sheet density and conduction area for the fixed bias current.

To quantify the performance of these micro-Hall sensors, we plotted absolute Hall sensitivity with respect to bias current, as shown in Fig. 7. As seen in Fig. 7, there is about 11% increase in absolute sensitivity from AlGaN/1.3-nm AlN/GaN to 20-nm QW micro-Hall device at room temperature.

A major point is that the 20-nm QW outperforms the AlGaN/1.3-nm AlN/GaN 2DEG Hall sensor using the same fabrication method. These techniques rely on decreasing the current carrying cross-sectional area and sheet density by reducing thickness to increase the drift velocity to enhance the Hall sensor signal for the same bias current and magnetic field.

Likewise, Fig. 8 shows the AlN/GaN/AlN QW Hall voltage versus temperature relationship in the range from −100 °C to 350 °C operating in the constant current mode. The removal

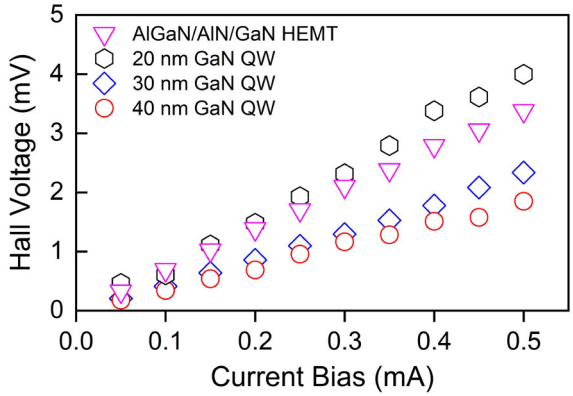

Fig. 6. Hall sensor signal for the 40-, 30-, and 20-nm QWs versus bias current in comparison with a reference AlGaN/1.3-nm AlN/GaN 2DEG Hall device for fixed 0.1-T magnetic field at room temperature.

of the offset voltage and measurement of the local temperature are accomplished using the same techniques described in our previous publication [20].

Based on parameters, such as temperature range, current scaled sensitivity (S_I), and temperature coefficient (S_I TC), Table I presents a comparison between GaN QW sensors and the state-of-the-art sensor technologies [12], [15], [36], [37], [38], [39], [40], [41].

Realizing that decreasing the bias current channel cross-sectional area increased the carrier velocity and Hall signal, we explored a new idea that relied on adding a gate to the Hall sensor at the precise spatial point of the Hall

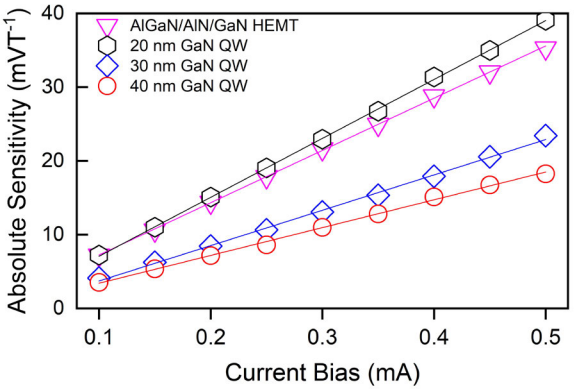

Fig. 7. Absolute sensitivity of the Hall sensor as a function of current bias.

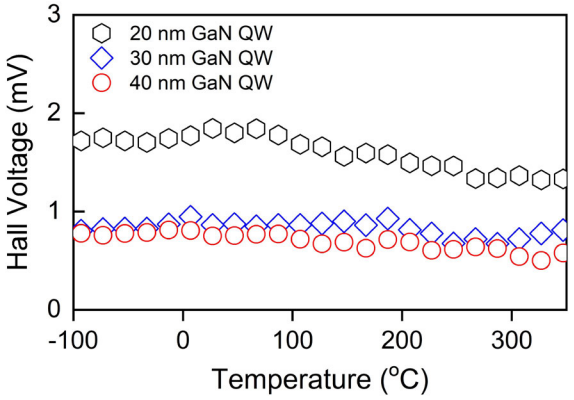

Fig. 8. AlN/GaN/AlN QW micro-Hall sensors show stable Hall voltage response for fixed 0.1-T magnetic field as a function of temperature under constant 0.2-mA bias current.

TABLE I
COMPARISON OF GaN QW HALL SENSOR WITH THE STATE-OF-THE-ART HIGH-TEMPERATURE HALL SENSOR

Hall Materials	Temperature Range (°C)	S_I at 25 °C ($VA^{-1}T^{-1}$)	Temperature Coefficient S_ITC (ppm/°C)	Refs
Si	-10 - 130	60	800	[36-39]
n-InSb/GaAs	-270 - 300	2	400	[40]
InAs/$Al_{0.2}Ga_{0.8}Sb$	-100 - 150	302	5780	[41]
AlGaAs/InGaAs/GaAs	-100 - 180	100	800	[12]
AlInSb/InAsSb/AlInSb	25 - 150	2540	13800	[15]
AlN/GaN/AlN (this work)	-113 - 350	92	720	

signal measurement, as shown in Fig. 9(a). By applying a gate voltage, we distribute the same applied voltage to be heavily weighted at the precise spatial point of the Hall signal measurement. Consequently, the electric field and carrier velocity are increased producing a higher Hall signal. This technique worked perfectly as seen by the enhancement in Hall voltage shown in Fig. 9(b) when a gate voltage is applied as indicated in Fig. 9(a). The measured Hall sensitivity for the gated Hall sensor shown in Fig. 9(b) yields a device sensitivity is 6.1 $VW^{-1}T^{-1}$, which is nearly twice the sensitivity of 3.6 $VW^{-1}T^{-1}$ observed without the gate voltage. We emphasize that this is with the constant Hall bias current or applied power.

Furthermore, the Schottky gate QW Hall sensor output Hall voltage versus applied magnetic field behavior for different bias currents ranging from 0.1 to 0.4 mA was measured,

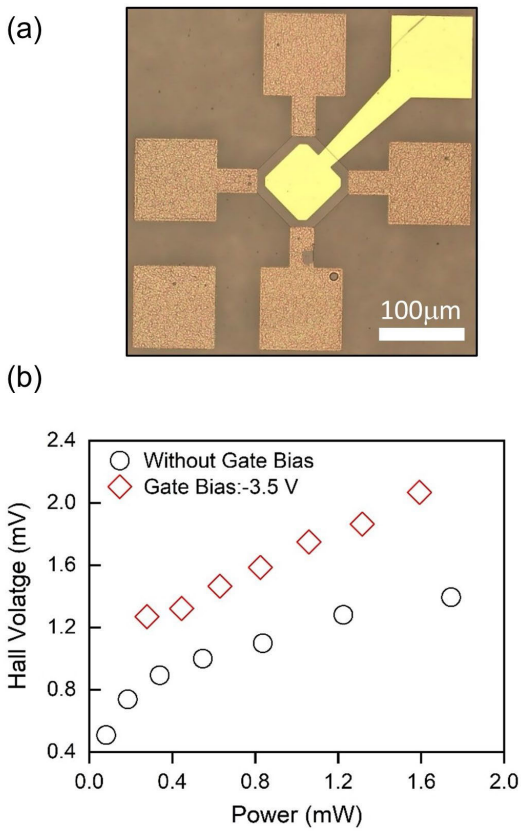

Fig. 9. (a) Hall sensor device (GaN QW thickness is 30 nm) with added Schottky gate to control the bias current flow cross-sectional area. (b) Comparison of Hall voltage for fixed 0.1-T magnetic field concerning without and with gate voltage in reference to applied power.

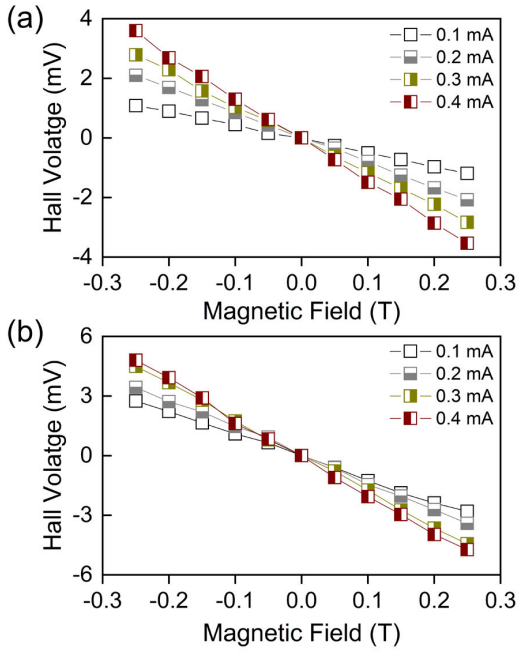

Fig. 10. (a) and (b) Hall sensor device (GaN QW thickness is 30 nm) with added Schottky gate have a linear response to magnetic field for without and with fixed gate voltage at room temperature.

as shown in Fig. 10. Fig. 10(a) presents the Hall voltage, which varies linearly with the applied magnetic field from −0.25 to 0.25 T without applying gate voltage. Fig. 10(b) depicts that the added gate voltage to the Schottky gate QW

Hall sensors shows higher Hall voltage and signal linearity for applied magnetic field from −0.25 to 0.25 T. This is consistent with the added restriction to the bias current by decreasing the effective thickness again only at the Hall voltage measurement point.

This is not an effect that depends simply on increasing the applied bias voltage, current, or power. Rather, the gate redistributes approximately the same applied voltage to take advantage of a higher electric field only at the site of the Hall measurement, while keeping the applied power to the device approximately the same [Fig. 9(b)]. Moreover, a much higher improvement in the Hall sensor sensitivity is possible by using a smaller lateral size for the gate electrode.

IV. Conclusion

In summary, we have grown several AlN/GaN/AlN heterostructures by MBE and fabricated Hall sensors. In comparison with standard AlGaN/AlN/GaN Hall sensors, we find that the AlN/GaN/AlN QW Hall sensors, for the same sensor geometry, have a higher sensitivity. In addition, we have demonstrated for the first time that the use of a gate can significantly increase the Hall sensitivity of any Hall device without a significant change in input power or applied voltage. This is because the gate voltage redistributes the bias voltage to produce a higher applied electric field only at precisely the Hall measurement site while keeping the device applied voltage and current approximately the same. The future direction of this research involves integrating a Hall sensor with a high-power transistor on the same chip to enable real-time monitoring of both current and temperature.

References

[1] H. Lu, P. Sandvik, A. Vertiatchikh, J. Tucker, and A. Elasser, "High temperature Hall effect sensors based on AlGaN/GaN heterojunctions," *J. Appl. Phys.*, vol. 99, no. 11, Jun. 2006, Art. no. 114510, doi: 10.1063/1.2201339.

[2] A. Kadechkar, J.-R. Riba, M. Moreno-Eguilaz, and J. Sanllehí, "Real-time wireless, contactless, and coreless monitoring of the current distribution in substation conductors for fault diagnosis," *IEEE Sensors J.*, vol. 19, no. 5, pp. 1693–1700, Mar. 2019, doi: 10.1109/JSEN.2018.2884566.

[3] A. Itzke, R. Weiss, and R. Weigel, "Influence of the conductor position on a circular array of Hall sensors for current measurement," *IEEE Trans. Ind. Electron.*, vol. 66, no. 1, pp. 580–585, Jan. 2019, doi: 10.1109/TIE.2018.2826462.

[4] A. Ajbl, M. Pastre, and M. Kayal, "A fully integrated Hall sensor microsystem for contactless current measurement," *IEEE Sensors J.*, vol. 13, no. 6, pp. 2271–2278, Jun. 2013, doi: 10.1109/JSEN.2013.2251971.

[5] N. Jankovic, O. Kryvchenkova, S. Batcup, and P. Igic, "High sensitivity dual-gate four-terminal magnetic sensor compatible with SOI FinFET technology," *IEEE Electron Device Lett.*, vol. 38, no. 6, pp. 810–813, Jun. 2017, doi: 10.1109/LED.2017.2693559.

[6] J. Lenz and S. Edelstein, "Magnetic sensors and their applications," *IEEE Sensors J.*, vol. 6, no. 3, pp. 631–649, Jun. 2006, doi: 10.1109/JSEN.2006.874493.

[7] M. Miyoshi et al., "High-electron-mobility AlGaN/AlN/GaN heterostructures grown on 100-mm-diam epitaxial AlN/sapphire templates by metalorganic vapor phase epitaxy," *Appl. Phys. Lett.*, vol. 85, no. 10, pp. 1710–1712, Sep. 2004, doi: 10.1063/1.1790073.

[8] P. G. Neudeck, D. J. Spry, L. Chen, N. F. Prokop, and M. J. Krasowski, "Demonstration of 4H-SiC digital integrated circuits above 800 °C," *IEEE Electron Device Lett.*, vol. 38, no. 8, pp. 1082–1085, Aug. 2017, doi: 10.1109/LED.2017.2719280.

[9] T. Yamamura, D. Nakamura, M. Higashiwaki, T. Matsui, and A. Sandhu, "High sensitivity and quantitative magnetic field measurements at 600 °C," *J. Appl. Phys.*, vol. 99, no. 8, pp. 1–4, Apr. 2006, doi: 10.1063/1.2158693.

[10] N. Maeda, K. Tsubaki, T. Saitoh, and N. Kobayashi, "High-temperature electron transport properties in AlGaN/GaN heterostructures," *Appl. Phys. Lett.*, vol. 79, no. 11, pp. 1634–1636, Sep. 2001, doi: 10.1063/1.1400779.

[11] A. Hassan, A. Mahar, K. A. Faruque, S. Shetty, G. J. Salamo, and H. A. Mantooth, "A fast interface circuit using multiple signal paths for high bandwidth Hall sensors," in *Proc. 20th IEEE Interregional NEWCAS Conf. (NEWCAS)*, Jun. 2022, pp. 218–221, doi: 10.1109/NEWCAS52662.2022.9842177.

[12] N. Haned and M. Missous, "Nano-Tesla magnetic field magnetometry using an InGaAs-AlGaAs-GaAs 2DEG Hall sensor," *Sens. Actuators A, Phys.*, vol. 102, no. 3, pp. 216–222, Jan. 2006, doi: 10.1016/S0924-4247(02)00386-2.

[13] T. Iwabuchi et al., "High sensitivity Hall elements made from Si-doped InAs on GaAs substrates by molecular beam epitaxy," *J. Cryst. Growth*, vol. 150, no. 94, pp. 1302–1306, 1995, doi: 10.1016/0022-0248(95)80149-7.

[14] V. P. Kunets et al., "Generation-recombination noise in doped-channel $Al_{0.3}Ga_{0.7}As/GaAs/In_{0.2}Ga_{0.8}As$ quantum well micro-Hall devices," *J. Appl. Phys.*, vol. 94, no. 12, pp. 7590–7593, Dec. 2003, doi: 10.1063/1.1625783.

[15] S. Koide, H. Takahashi, A. Abderrahmane, I. Shibasaki, and A. Sandhu, "High temperature Hall sensors using AlGaN/GaN HEMT structures," *J. Phys., Conf. Ser.*, vol. 352, Mar. 2012, Art. no. 012009, doi: 10.1088/1742-6596/352/1/012009.

[16] G. Brezeanu et al., "High temperature sensors based on silicon carbide (SiC) devices," in *Proc. Int. Semiconductor Conf. (CAS)*, Oct. 2015, pp. 3–10, doi: 10.1109/SMICND.2015.7355147.

[17] J. Singhal et al., "AlN/AlGaN/AlN quantum well channel HEMTs," *Appl. Phys. Lett.*, vol. 122, no. 22, May 2023, Art. no. 222106, doi: 10.1063/5.0145582.

[18] E. Kim et al., "N-polar GaN/AlGaN/AlN high electron mobility transistors on single-crystal bulk AlN substrates," *Appl. Phys. Lett.*, vol. 122, no. 9, Feb. 2023, Art. no. 092104, doi: 10.1063/5.0138939.

[19] H. Amano et al., "The 2018 GaN power electronics roadmap," *J. Phys. D, Appl. Phys.*, vol. 51, no. 16, Apr. 2018, Art. no. 163001, doi: 10.1088/1361-6463/aaaf9d.

[20] T. P. White, S. Shetty, M. E. Ware, H. A. Mantooth, and G. J. Salamo, "AlGaN/GaN micro-Hall effect devices for simultaneous current and temperature measurements from line currents," *IEEE Sensors J.*, vol. 18, no. 7, pp. 2944–2951, Apr. 2018, doi: 10.1109/JSEN.2018.2794264.

[21] S. Shetty et al., "Thermal stability study of gallium nitride based magnetic field sensor," *J. Appl. Phys.*, vol. 134, no. 14, Oct. 2023, Art. no. 145303, doi: 10.1063/5.0156013.

[22] A. Krone et al., "High temperature degradation modes observed in gallium nitride-based Hall-effect sensors," *J. Electron. Packag.*, vol. 144, no. 2, pp. 1–8, Jun. 2022, doi: 10.1115/1.4053765.

[23] A. Krone, H. Alpert, S. Shetty, D. G. Senesky, G. Salamo, and D. Huitink, "Degradation of gallium nitride-based Hall-effect sensors in high temperature environments," in *Proc. ASME Int. Tech. Conf. Exhib. Packag. Integr. Electron. Photonic Microsystems*, Oct. 2020, pp. 1–10, doi: 10.1115/IPACK2020-2589.

[24] S. C. Jain, M. Willander, J. Narayan, and R. V. Overstraeten, "III-nitrides: Growth, characterization, and properties," *J. Appl. Phys.*, vol. 87, no. 3, pp. 965–1006, Feb. 2000, doi: 10.1063/1.371971.

[25] I. P. Smorchkova et al., "AlN/GaN and (Al,Ga)N/alN/GaN two-dimensional electron gas structures grown by plasma-assisted molecular-beam epitaxy," *J. Appl. Phys.*, vol. 90, no. 10, pp. 5196–5201, Nov. 2001, doi: 10.1063/1.1412273.

[26] G. Li et al., "Two-dimensional electron gases in strained quantum wells for AlN/GaN/AlN double heterostructure field-effect transistors on AlN," *Appl. Phys. Lett.*, vol. 104, no. 19, May 2014, Art. no. 193506, doi: 10.1063/1.4875916.

[27] M. Qi et al., "Strained GaN quantum-well FETs on single crystal bulk AlN substrates," *Appl. Phys. Lett.*, vol. 110, no. 6, Feb. 2017, Art. no. 063501, doi: 10.1063/1.4975702.

[28] A. Y. Polyakov et al., "Electrical and structural properties of AlN/GaN and AlGaN/GaN heterojunctions," *J. Appl. Phys.*, vol. 104, no. 5, Sep. 2008, Art. no. 053702, doi: 10.1063/1.2973463.

[29] I. P. Smorchkova et al., "Two-dimensional electron-gas AlN/GaN heterostructures with extremely thin AlN barriers," *Appl. Phys. Lett.*, vol. 77, no. 24, pp. 3998–4000, Dec. 2000, doi: 10.1063/1.1332408.

[30] Y. Cao and D. Jena, "High-mobility window for two-dimensional electron gases at ultrathin AlN/GaN heterojunctions," *Appl. Phys. Lett.*, vol. 90, no. 18, Apr. 2007, Art. no. 182112, doi: 10.1063/1.2736207.

[31] F. Machuca, Z. Liu, Y. Sun, P. Pianetta, W. E. Spicer, and R. F. W. Pease, "Simple method for cleaning gallium nitride (0001)," *J. Vac. Sci. Technol. A, Vac., Surf., Films*, vol. 20, no. 5, pp. 1784–1786, Sep. 2002, doi: 10.1116/1.1503782.

[32] C.-T. Liang et al., "Huge positive magnetoresistance in an InN film," *Appl. Phys. Lett.*, vol. 90, no. 17, pp. 1–4, Apr. 2007, doi: 10.1063/1.2730755.
[33] M. Diale, F. D. Auret, N. G. van der Berg, R. Q. Odendaal, and W. D. Roos, "Analysis of GaN cleaning procedures," *Appl. Surf. Sci.*, vol. 246, nos. 1–3, pp. 279–289, Jun. 2005, doi: 10.1016/j.apsusc.2004.11.024.
[34] Y. Cho et al., "Molecular beam homoepitaxy on bulk AlN enabled by aluminum-assisted surface cleaning," *Appl. Phys. Lett.*, vol. 116, no. 17, Apr. 2020, Art. no. 172106, doi: 10.1063/1.5143968.
[35] M. Qi et al., "Dual optical marker Raman characterization of strained GaN-channels on AlN using AlN/GaN/AlN quantum wells and 15N isotopes," *Appl. Phys. Lett.*, vol. 106, no. 4, Jan. 2015, doi: 10.1063/1.4906900.
[36] G. S. Randhawa, "Monolithic integrated Hall devices in silicon circuits," *Microelectron. J.*, vol. 12, no. 6, pp. 24–29, Nov. 1981, doi: 10.1016/S0026-2692(81)80360-6.
[37] S. R. In't Hout and S. Middelhoek, "A 400 °C silicon Hall sensor," *Sens. Actuators A, Phys.*, vol. 60, nos. 1–3, pp. 14–22, May 1997.
[38] U. Ausserlechner, "Hall effect devices with three terminals: Their magnetic sensitivity and offset cancellation scheme," *J. Sensors*, vol. 2016, pp. 1–16, Jan. 2016, doi: 10.1155/2016/5625607.
[39] U. Ausserlechner, "Closed form expressions for sheet resistance and mobility from Van-der-Pauw measurement on 90° symmetric devices with four arbitrary contacts," *Solid-State Electron.*, vol. 116, pp. 46–55, Feb. 2016, doi: 10.1016/j.sse.2015.11.030.
[40] J. Jankowski, S. El-Ahmar, and M. Oszwaldowski, "Hall sensors for extreme temperatures," *Sensors*, vol. 11, no. 1, pp. 876–885, Jan. 2011, doi: 10.3390/s110100876.
[41] M. Behet, J. Bekaert, J. De Boeck, and G. Borghs, "InAs/$Al_{0.2}Ga_{0.8}Sb$ quantum well Hall effect sensors," *Sens. Actuators A, Phys.*, vol. 81, nos. 1–3, pp. 13–17, Apr. 2000.

Satish Shetty received the Ph.D. degree from the Jawaharlal Nehru Centre for Advanced Scientific Research (JNCASR), Bengaluru, India, in 2014.

He is currently a Postdoctoral Research Fellow with the University of Arkansas, Fayetteville, AR, USA. His research interests include designing and developing innovative sensors, HEMTs for harsh environmental applications, growing low-dimensional semiconductor nanostructures and heterostructures using MBE, fabrication of electronic-optoelectronic device using electron beam lithography, photolithography, dry (ICP) and wet etching process, PECVD, and device characterization.

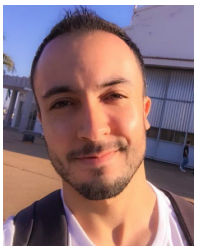

Fernando Maia de Oliveira received the Ph.D. degree in physics from the Federal University of Sao Carlos, São Paulo, Brazil, in 2021.

He is currently a Research Assistant with the Institute for Nanoscience and Engineering, University of Arkansas, Fayetteville, AR, USA. His research interests include the Raman scattering of semiconductors, with emphasis on III-nitride nanomaterials.

Yuriy I. Mazur received the M.Sc. degree in solid state physics from the Moscow Institute of Physics and Engineering, Moscow, Russia, in 1978, and the Ph.D. degree in solid state physics from the Institute of General Physics, Moscow, in 1983.

He was with the Institute of Semiconductors Physics, National Academy of Sciences, Kiev, Ukraine, and the Max-Born-Institute, Berlin, Germany, as a Senior Research Associate and a Visiting Scientist, from 1982 to 2000. He joined the Department of Physics, University of Arkansas, Fayetteville, AR, USA, in 2001. He is currently a Research Professor with the Institute for Nanoscience and Engineering, University of Arkansas. His research interests include physics of magnetic phenomena and disordering in the semi-magnetic semiconductors, physics of 2-D electron (hole) states, and excitons in III–V semiconductor heterostructures and quantum dots.

H. Alan Mantooth (Fellow, IEEE) received the B.S.E.E. and M.S.E.E. degrees from the University of Arkansas, Fayetteville, AR, USA, in 1985 and 1986, respectively, and the Ph.D. degree from the Georgia Institute of Technology, Atlanta, GA, USA, in 1990.

He then joined Analogy, a startup company in Oregon, where he focused on semiconductor device modeling and the research and development of modeling tools and techniques. In 1998, he joined the faculty of the Department of Electrical Engineering at the University of Arkansas, where he currently holds the rank of Distinguished Professor and holds the 21st Century Research Leadership Chair in Engineering. Dr. Mantooth leads the UA Power Group as Executive Director, which is a multidisciplinary, vertically-integrated power electronics program that includes MUSiC, HiDEC, and NCREPT as core facilities for SiC device and circuit fabrication, advanced power module packaging, and high-power test, respectively. Dr. Mantooth has led the establishment of the National Multi-User Silicon Carbide Fabrication Facility (MUSiC) and the National Center for Reliable Electric Power Transmission (NCREPT) at the UA. He also serves as the Founding Director of the NSF Industry/University Cooperative Research Center on GRid-connected Advanced Power Electronic Systems (GRAPES). In 2015, he also helped to establish the UA's first NSF Engineering Research Center entitled Power Optimization for Electro-Thermal Systems (POETS) that focuses on high power density systems for electrified transportation applications. Dr. Mantooth has co-founded three companies in design automation (Lynguent), IC design (Ozark Integrated Circuits), and cybersecurity (Bastazo) as well as advising a fourth in power electronics packaging (Arkansas Power Electronics International) to maturity and acquisition as a board member. He also serves as Division II Director-Elect (2024) and Director (2025-26) on the IEEE Board of Directors. His research interests now include analog and mixed-signal IC design & CAD, semiconductor device modeling, power electronics, power electronics packaging, and cybersecurity.

Dr. Mantooth is a Past-President for the IEEE Power Electronics Society and currently serves as Editor-in-Chief of the IEEE *Open Journal of Power Electronics*. Dr. Mantooth is a member of Tau Beta Pi, Sigma Xi, and Eta Kappa Nu, and registered professional engineer in Arkansas.

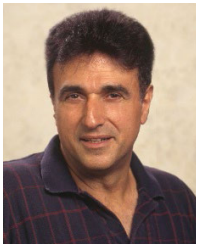

Gregory J. Salamo received the Ph.D. in physics from the City University of New York, New York, NY, USA, in 1973.

He holds the Basore Chair in Nanotechnology and Innovation. where he also worked as an intern student at Bell Laboratories, Murray Hill, New Jersey, from 1968 to 1973. His Postdoctoral work was at the Institute of Optics of University of Rochester, New York, from 1973 to 1975. He joined the faculty of the University of Arkansas in January of 1975, where he is now Distinguished Professor of Physics and the Basore Professor in Nanotechnology and Innovation. He also pursues the development of interdisciplinary research and education through the establishment of a new MS/Ph.D. degree program first called Micro Electronics-Photonics but now Material Science and Engineering, which is now the home of over 80 graduate students and provides greater career opportunities for students and faculty in the sciences. He has carried out research in the areas of optical spatial solitons, quantum optics, and the optical properties of semiconductors. He has published about 600 papers in referred journals, given numerous contributed and invited talks, contributed several conference proceedings and book chapters, and is editor of Springer Lecture Notes in Nanoscience. His research is currently focused on growing III-V and group IV semiconductors and ferroelectrics using molecular beam epitaxy (MBE), scanning tunneling microscopy (STM), and transmission electron microscopy (TEM). He has also started new laboratory courses in Laser Physics, Quantum Optics, Nonlinear Optics, Optic Communications, Optical Properties of Solids, and Nanoscale Fabrication and Imaging, each with separate NSF Awards.

Dr. Salamo is a Fellow of the Optical Society of America and the American Physical Society and won the UA Baum Award for Teaching, the most prestigious UA award made to one faculty member each year. He was also the 2009 Case Professor of the Year.